J Mater Sci (2017) 52:13841–13851

Computation

Electronic and optical properties of the wurtzite-ZnO/$CH_3NH_3PbI_3$ interface: first-principles calculations

Fengjuan Si[1], Wei Hu[2], Fuling Tang[1,3,*], Yuwen Cheng[1], and Hongtao Xue[1]

[1] Department of Materials Science and Engineering, State Key Laboratory of Advanced Processing and Recycling of Non-ferrous Metals, Lanzhou University of Technology, Lanzhou 730050, China
[2] Department of Materials Engineering, Lanzhou Institute of Technology, Lanzhou 730050, China
[3] Department of Chemistry, Texas A&M University, 700 Univ Blvd, Kingsville, TX 78363, USA

Received: 15 December 2016
Accepted: 6 June 2017
Published online:
7 September 2017

© Springer Science+Business Media, LLC 2017

ABSTRACT

The atomistic geometry, binding energy, optical and electronic properties of wurtzite-ZnO (WZ-ZnO) (100)/$CH_3NH_3PbI_3$ ($MAPbI_3$) (112) interface were studied with the first-principles calculations. The lattice mismatch of this interface is 8.9%, and the interface binding energy is -0.164 J/m^2. Interface states appear nearby the Fermi level, which come from the contribution of O-2*p* orbital, I-5*p* orbital and Pb-6*s* orbital. The atom orbitals of WZ-ZnO (100)/$MAPbI_3$ (112) interface have hybridizations. Through the analysis of charge density difference and Bader atomic charges, it is found that there is obvious charge transfer at the interface.

Introduction

High efficiency and low cost are two key factors for research and development of the large-scale application of solar photovoltaic technology [1–4]. Recently, hybrid organic–inorganic perovskite solar cells have attracted much attention between academia and industrial circles owing to their high efficiency, easy to prepare and low cost [5–7]. Perovskite solar cells are multilayer devices [8], and the typical structure of perovskite solar cells is: conducting glass | electron transporting layer | light-absorbing layer | hole transporting layer | metal electrode. Electron transporting material can be TiO_2 [9], ZnO [10], C60 [11], etc. Light-absorbing material can be $CH_3NH_3PbI_3$ ($MAPbI_3$) [12], $CH_3NH_3PbI_{3-x}Cl_x$ [13], $CH_3NH_3PbBr_3$ [14], etc. Hole transporting material can be spiro-OMeTAD [12], NiO [15], 2TPA-2-DP [16], etc. Multilayer structure is the physical basis of the photovoltaic effects [17]. Photoelectric performance of perovskite solar cells not only depends on the chemical composition, properties and morphology of the material in each layer but also depends on the structure and properties of interface, because interface is a major place for charge extracting, transporting and recombination.

Recently, some researchers had focused on the interfaces of perovskite solar cells, and they had studied some interfaces of perovskite solar cells. The origin of thermal instability on $MAPbI_3$/ZnO interface was studied with the first-principles calculations and X-ray diffraction (XRD) by Yang et al. [18]. They

Address correspondence to E-mail: tfl03@mails.tsinghua.edu.cn

DOI 10.1007/s10853-017-1276-2

found that the presence of hydroxyl accelerated the decomposition process. Zhou et al. [19] studied electronic properties of the $MAPbI_3$/WZ-ZnO (0001) interface using ultraviolet photoelectron spectroscopy and XRD. They found that the electrons are transferred from $MAPbI_3$ to ZnO, while the holes can be blocked. Zhang et al. [20] studied perovskite solar cells with ITO/ZnO/$MAPbI_3$/spiro-OMeTAD/AgNWs structure. The device showed the highest power conversion efficiency (PCE) of 9.21%. Zhou et al. [21] studied perovskite solar cells with ZnO/$MAPbI_3$/C structure, and the device had PCE of 8%. Song et al. [22] used XRD and scanning electron microscope (SEM) technology to investigate the photovoltaic performance of ITO/ZnO film, ITO/ZnO/$MAPbI_3$ film and ITO/ZnO/$MAPbI_3$/HTM film. It was found that the thickness of ZnO layer was a key parameter to determine the photovoltaic performance. Liu et al. [10] used ZnO as electron-transport layer to construct perovskite solar cells. Compared with perovskite solar cells with TiO_2 as electron-transport layer, annealing temperature of ZnO layer is lower and the perovskite solar cells with PCE in excess of 10% [23]. It is difficult to directly observe the microstructure of the interface at atomistic level by experimental methods. So a theoretical investigation is needed. In this paper, we employ first-principles method to study electronic and optical properties of WZ-ZnO (100)/$MAPbI_3$ (112) interface. We investigate the density of states (DOS), charge density difference and Bader charge on WZ-ZnO/$MAPbI_3$ interface. Then we calculated the optical properties (including absorption coefficient, refractive indices and extinction coefficient) of $MAPbI_3$ bulk, $MAPbI_3$ (112) surface and WZ-ZnO/$MAPbI_3$ interface, respectively. The aim of our research is to construct the WZ-ZnO/$MAPbI_3$ interface models, to deeply understand the electrical and optical properties of WZ-ZnO/$MAPbI_3$ interface.

Methods

We use the *Vienna* ab initio *simulation* package (VASP) as the simulation platform [24–26]. VASP is based on first-principles density functional theory (DFT) with Perdew–Burke–Ernzerhof (PBE) [27] version of the generalized gradient approximation (GGA). The projector augmented wave (PAW) [28, 29] method is applied to describe the pseudopotential. The electron configurations of hydrogen, carbon, nitrogen, iodine, plumbum, zinc, oxygen are H$1s^1$, C$2s^22p^2$, N$2s^22p^3$, [Kr]$5s^25p^5$, [Xe]$5d^{10}6s^26p^2$, [Ar]$3d^{10}4s^2$, O$2s^22p^4$, respectively. The cutoff energy of WZ-ZnO bulk, $MAPbI_3$ bulk, WZ-ZnO (100) surface, $MAPbI_3$ (112) surface, WZ-ZnO (100)/$MAPbI_3$ (112) interface is 550 eV. *K*-points gamma-centered meshes are 7 × 7 × 4 and 4 × 4 × 4 for calculating for WZ-ZnO and $MAPbI_3$ bulk, respectively. *K*-points meshes are done with 1 × 2 × 2 for calculating WZ-ZnO (100) and $MAPbI_3$ (112) surface, and *K*-points meshes are done with 2 × 2 × 1 for calculating WZ-ZnO (100)/$MAPbI_3$ (112) interface.

Almost all of the optical properties of materials can be deduced from DFT calculated complex dielectric function. The optical properties mainly refer to the absorption coefficient, refractive indices and extinction coefficient and so on. The optical properties of WZ-ZnO/$MAPbI_3$ interface are expressed by the terms of the dielectric functions $\varepsilon(\omega)$ (1) and absorption coefficient $\alpha(\omega)$ (2). The imaginary part $\varepsilon^{(2)}_{\alpha\beta}(\omega)$ is determined by a summation over empty states using Eq. (3), and the real part $\varepsilon^{(1)}_{\alpha\beta}(\omega)$ of the dielectric tensor is obtained by the usual Kramers–Kronig transformation [30] using Eq. (4)

$$\varepsilon(\omega) = \varepsilon_1(\omega) + i\varepsilon_2(\omega) \tag{1}$$

$$\alpha(\omega) = \sqrt{2}\omega\left[\sqrt{\varepsilon_1(\omega)^2 + \varepsilon_2(\omega)^2} - \varepsilon_1(\omega)\right]^{1/2} = 2\omega\kappa \tag{2}$$

$$\begin{aligned}\varepsilon^{(2)}_{\alpha\beta}(\omega) = \frac{4e^2\pi^2}{\Omega}\lim_{q\to 0}\frac{1}{q^2}\sum_{c,v,k} 2w_k\delta(\varepsilon_{ck} - \varepsilon_{vk} - \omega) \\ \times \langle u_{ck} + e_{\alpha q}|u_{vk}\rangle\langle u_{ck} + e_{\beta q}|u_{vk}\rangle^*\end{aligned} \tag{3}$$

$$\varepsilon^{(1)}_{\alpha\beta}(\omega) = 1 + \frac{2}{\pi}P\int_0^\infty \frac{\varepsilon^{(2)}_{\alpha\beta}(\omega')\omega'}{\omega'^2 - \omega^2 + i\eta}d\omega' \tag{4}$$

Here, c and v are conduction and valence band states, respectively, and u_{ck} is the cell periodic part of the wavefunctions at the *k*-point k. P is the principle value. η is infinitesimal number.

There are many methods to describe the electron distribution in DFT simulation. Both Mulliken population analysis [31] and Bader population analysis [32] are more popular. They are very convenient to analyze the valence of each atom and the gain and loss of electrons in the system using the population analysis. Mulliken analysis divides overlap populations equally between the two atoms of a bond and

thus has the advantage of simplicity. However, its results tend to vary with the basis sets employed and it yields unnatural values in some cases. In this work, Bader population analysis is used to deal with atomic charge, thus to analyze valence change and the gain and loss of electron number. Henkelman [33] provides Bader charge analysis method; it is only limited to describe the system calculated by atomic pseudopotential method with the plane wave projection (PAW). To a certain extent, both charge density waves and charge density difference can express the net change distribution of the charge in the whole space. In this work, charge density difference is used to figure out the electronic distribution of the interface based on VASETA [34].

Results and discussion

Geometry of WZ-ZnO and $MAPbI_3$ bulk

We investigate the lattice structures of WZ-ZnO and $MAPbI_3$ bulk, and choose the wurtzite-ZnO and cubic perovskite structure $MAPbI_3$ to build the interface model. The calculated lattice parameters of WZ-ZnO are $a = b = 3.25$, $c = 5.21$ Å, while other calculated values are $a = b = 3.285$, $c = 5.262$ Å [35]. For cubic $MAPbI_3$, our calculated lattice parameters are $a = b = c = 6.33$ Å. Compared with experiment value 6.295 Å [36–39], our optimized value is reliable. For the WZ-ZnO (100) and $MAPbI_3$ (112) surface, we build six-layer slabs to simulate their surfaces. Figure 1 shows the surface model: The bottom three layers are fixed to represent the bulk, and the top three layers are relaxed representing the surface. For WZ-ZnO (100) surface model, the lattice parameters are $a = 10.41$, $b = 9.75$, $c = 18.44$ Å. The model has 6 atomic layers, and there are 6 Zn atoms and 6 O atoms on each layer. For $MAPbI_3$ (112) surface model, the lattice parameters are $a = 10.96$, $b = 8.95$, $c = 31.80$ Å, it also includes 6 atoms layers, and there are 12 atoms which there are 1 C atom, 1 N atom, 1 Pb atom, 3 I atoms and 6 H atoms on each layer. For eliminating effects of periodic boundary conditions on the surface model, we add 12 and 4 passivation H atoms at the bottom of WZ-ZnO and $MAPbI_3$, respectively. We add a 20 Å vacuum layer for the top of each surface model. After checking different crystal planes of WZ-ZnO and $MAPbI_3$, it is found that WZ-Zn (100) and $MAPbI_3$ (112) surfaces can make lattice match. Figure 2 shows the lattice mismatch of WZ-ZnO (100)/$MAPbI_3$ (112) surfaces. The lattice mismatch of WZ-ZnO (100)/$MAPbI_3$ (112) interface is about 8.9%. The tetrahedron method with Bloch corrections [40, 41] had been adopted for calculating density of states (DOS) of bulk, surface and interface model. We had used this method to study the interface of WZ-ZnO/CdS [35], Cu_2ZnSnS_4/WZ-ZnO [42], WZ-$CuInS_2$/WZ-CdS [43], indicating that the first-principles calculation methods are reliable.

Geometry of WZ-ZnO (100)/$MAPbI_3$ (112) interface

We build WZ-ZnO (100)/$MAPbI_3$ (112) interface model in Fig. 3. The interface model is divided into two parts. The left part has 6 single atomic layers of WZ-ZnO (100) plane, and the right part has 6 double

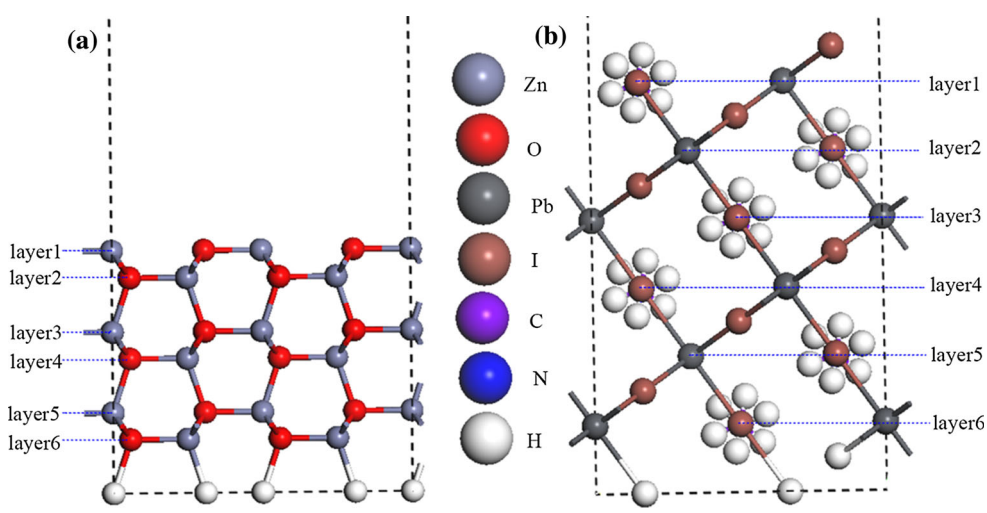

Figure 1 The surface model of WZ-ZnO (100) (**a**), $MAPbI_3$ (112) (**b**).

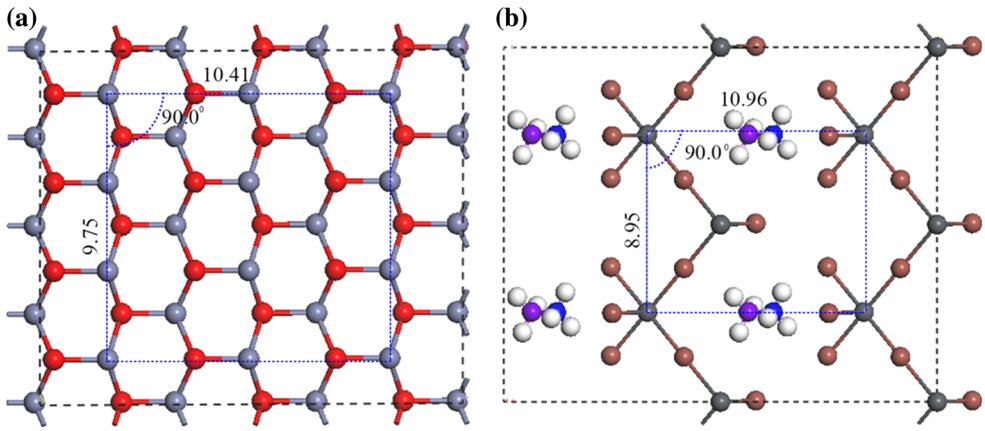

Figure 2 The lattice mismatch of WZ-ZnO (100) (**a**)/$MAPbI_3$ (112) (**b**) interface (Å).

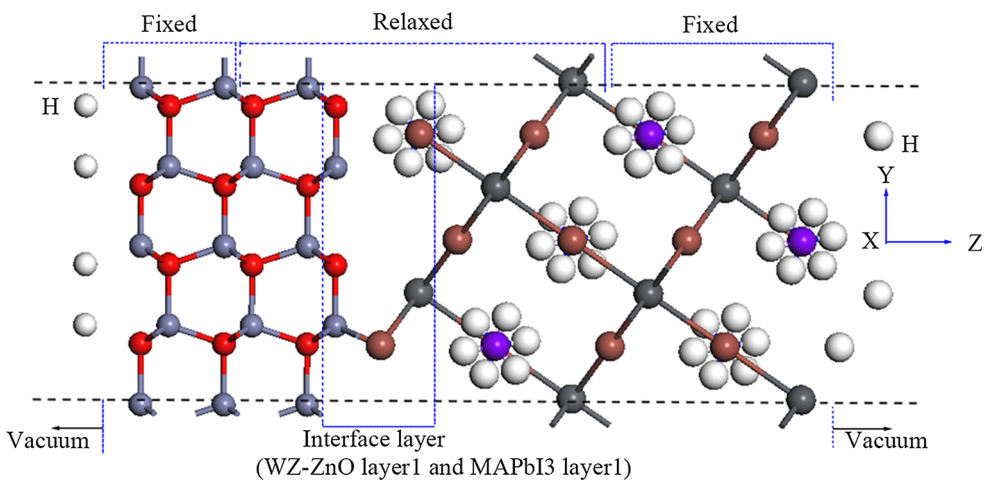

Figure 3 WZ-ZnO (100)/$MAPbI_3$ (112) interface model.

atomic layers of $MAPbI_3$ (112) plane. For eliminating effects of surface dangling bonds on the interfacial properties, we add 12 and 4 passivation hydrogen atoms on WZ-ZnO (100) surface and $MAPbI_3$ (100) surface, respectively. The lattice parameters of WZ-ZnO (100)/$MAPbI_3$ (112) interface are $a = 10.69$, $b = 9.35$, $c = 51.14$ Å. This interface model includes 36 Zn atoms, 36 O atoms, 6 N atoms, 6 C atoms, 6 Pb atoms, 18 I atoms, 36 H atoms and 16 passivation H atoms. In the model, we add 30 Å thickness vacuum layer to eliminate the effects of the surface atoms with periodic boundary conditions. We find suitable interface distance by single-point energy calculation. It is found that when the interface distance is 2.582 Å, the model system has the lowest total energy −636.05 eV, as shown in Fig. 4.

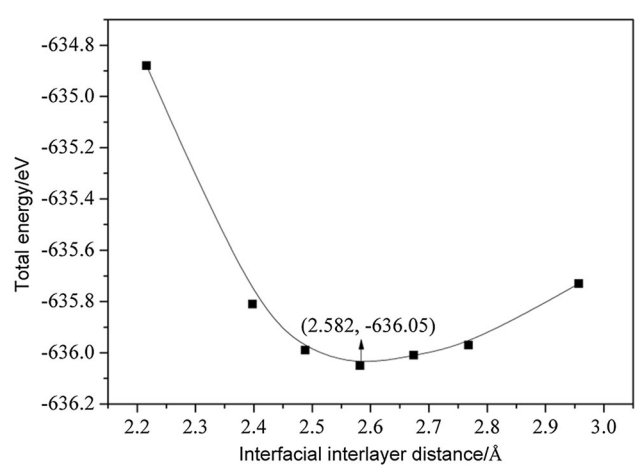

Figure 4 The total energy of the interface varies with the interface distance.

Interface binding energy of WZ-ZnO (100)/$MAPbI_3$ (112)

The interface binding energy can be considered as a criterion to judge stability of the WZ-ZnO (100)/

$MAPbI_3$ (112) interface. If the interface binding energy is negative, we think that the interface model is stable. Equation (5) is used to evaluate interface binding energy of WZ-ZnO (100)/$MAPbI_3$ (112)

$$E_{\text{ads}}\left(\text{eV}/\text{Å}^2\right) = \left[E_{\text{WZ-ZnO/MAPbI3}}\,(\text{eV}) - E_{\text{WZ-ZnO}}\,(\text{eV}) - E_{\text{MAPbI3}}\,(\text{eV})\right]/2S$$

The $E_{\text{WZ-ZnO/MAPbI3}}$ is the total energy of the whole system after relaxation. $E_{\text{WZ-ZnO}}$ or E_{MAPbI3} represents the isolated system energy of the interface model after relaxation, respectively. The $E_{\text{WZ-ZnO}}$ or E_{MAPbI3} part is kept, and E_{MAPbI3} or $E_{\text{WZ-ZnO}}$ is replaced by the vacuum. It is found that interface binding energy of WZ-ZnO (100)/$MAPbI_3$ (112) is $-0.164\ \text{J/m}^2$. The value of this interface binding energy is smaller than those of WZ-ZnO/CdS [35], Cu_2ZnSnS_4/WZ-ZnO [42] and WZ-$CuInS_2$/WZ-CdS [43], which are −0.61, −0.21 and $-0.68\ \text{J/m}^2$, respectively. This indicates that WZ-ZnO/$MAPbI_3$ is a somewhat weak interface.

Optical properties of WZ-ZnO (100)/$MAPbI_3$ (112) interface

Optical properties of $MAPbI_3$ are important to understand this absorption-layer material. The absorption coefficient α is the distance of a certain wavelength of light in the material before being fully absorbed. The absorption can occur only when the photon energy is greater than the band gap of the material. This is because the electrons of valence band can be excited to the conduction band by absorbing photons. When the photon energy is less than the band gap of the material, photons will not be absorbed. As shown in Fig. 5, it can be seen that optical band gap of the bulk $MAPbI_3$ is about 1.81 eV, which is very close to the reported values 1.62 eV [44] and 1.65 eV [45]. Absorption edge of the $MAPbI_3$ bulk is about 1.6 eV, which is higher than the experimental value of 1.5 eV and is also higher than the calculated result (<1.0 eV) based on SOC–GW [46]. The absorption threshold of the $MAPbI_3$ (112) surface and WZ-ZnO/$MAPbI_3$ interface shifts to low energy (<0.5 eV). When photon energy is about 4.5 eV, the absorption coefficient α of the $MAPbI_3$ bulk reaches a peak value. The absorption coefficient α of $MAPbI_3$ surface has a similar tendency with that of the $MAPbI_3$ bulk, while the absorption coefficient α of $MAPbI_3$ surface decreases accordingly. This may be because the surface periodicity is destroyed and the unsaturated bonds are formed. For the absorption coefficient α of $MAPbI_3$ interface, there are two absorption peaks at about 1.8 and 3.3 eV. From the analysis of density of states (Fig. 7), the absorption peak (at 1.8 eV) of the $MAPbI_3$ interface corresponds to the electrons from the valence O-2*p* orbitals transition conduction band Pb-6*p* orbitals. For the absorption peak at 3.3 eV, it can be attributed to electrons from valence band of I-5*p* or Pb-6*s* orbitals transition conduction band of Pb-6*p* orbitals. When photon energy is less than 3.3 eV, the absorption coefficient α of WZ-ZnO/$MAPbI_3$ interface is slightly larger than that of the $MAPbI_3$ (112) surface. It can be seen that there are some hybridizations of Zn-3*d* orbital and O-2*p* orbital or hybridizations of O-2*p* orbital, I-5*p* orbital, Pb-6*s* orbital with Pb-6*p* orbital.

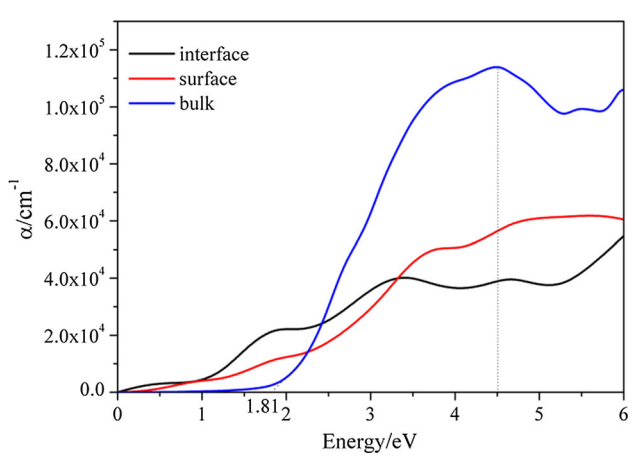

Figure 5 The absorption coefficient α of $MAPbI_3$ bulk, $MAPbI_3$ (112) surface, WZ-ZnO (100)/$MAPbI_3$ (112) interface.

Refractive indices n and extinction coefficient k are real part and imaginary part of complex refractive index N, respectively, $N = \sqrt{\varepsilon(\omega)} = n + ik$. As shown in Fig. 6a, refractive indices n of the $MAPbI_3$ bulk exhibit a major peak, which is located at 2.5 eV. Refractive indices n of the $MAPbI_3$ bulk show good agreement with previous reports [45]. But our calculated n of the $MAPbI_3$ bulk is less than other reported value; the trend of n curve of the surface $MAPbI_3$ (112) and WZ-ZnO/$MAPbI_3$ interface is consistent with other reported result from $MAPbI_3$ bulk [47]. Refractive indices n of the $MAPbI_3$ surface and WZ-ZnO/$MAPbI_3$ interface are less than that of the $MAPbI_3$ bulk at about 0.5–4.5 eV. From Fig. 6b, it can be seen that extinction coefficient k of the $MAPbI_3$ bulk increases first and then decreases. When photon

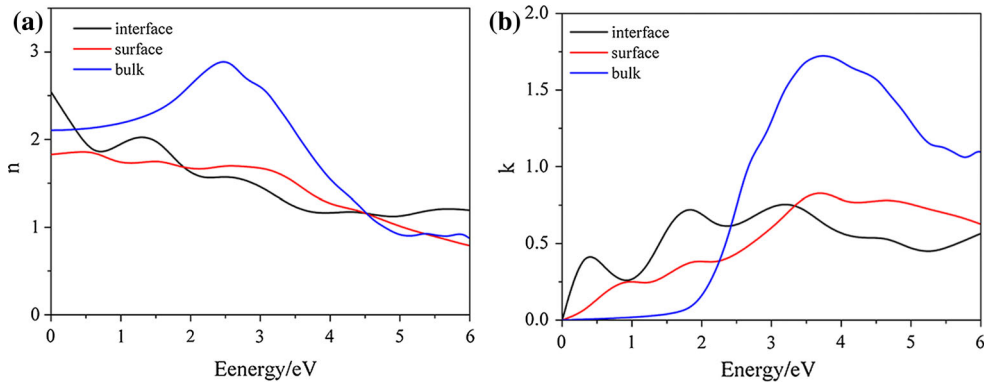

Figure 6 The refractive indices n and extinction coefficient k of $MAPbI_3$ bulk, $MAPbI_3$ (112) surface, WZ-ZnO (100)/$MAPbI_3$ (112) interface.

energy is less than 3.3 eV, the extinction coefficient k of WZ-ZnO/$MAPbI_3$ interface is greater than that of the surface $MAPbI_3$ (112). At present, to directly obtain the optical properties of the WZ-ZnO/$MAPbI_3$ interface from experiments is a hard task, so we hoped that our calculations can provide a theoretical reference value for them.

The electronic properties of WZ-ZnO (100)/ $MAPbI_3$ (112) interface

We study electronic properties of WZ-ZnO (100)/ $MAPbI_3$ (112) interface, including total density of states (TDOS), local density of states (LDOS), partial density of states (PDOS), charge density difference and Bader charge of the interface.

Figure 7a shows TDOS of WZ-ZnO (100)/$MAPbI_3$ (112) interface; the new electronic states can be seen nearby the Fermi level. When these two semiconductor materials form the heterojunction, the periodical structure of the crystal is damaged at the interface, so there are some additional interface levels in the band gap between the conduction band and valence band. These new electronic states (additional levels in the band gap) are interface states. Figure 7b, c shows LDOS of the WZ-ZnO (100) layer 5 and layer 1, the LDOS of WZ-ZnO (100) layer 5 represents that of the bulk WZ-ZnO. Through analyzing LDOS of the WZ-ZnO (100) layer 5 and WZ-ZnO (100) layer 1, we find that WZ-ZnO (100) layer 1 has some new energy densities states from −0.5 to 0.3 eV near the Fermi

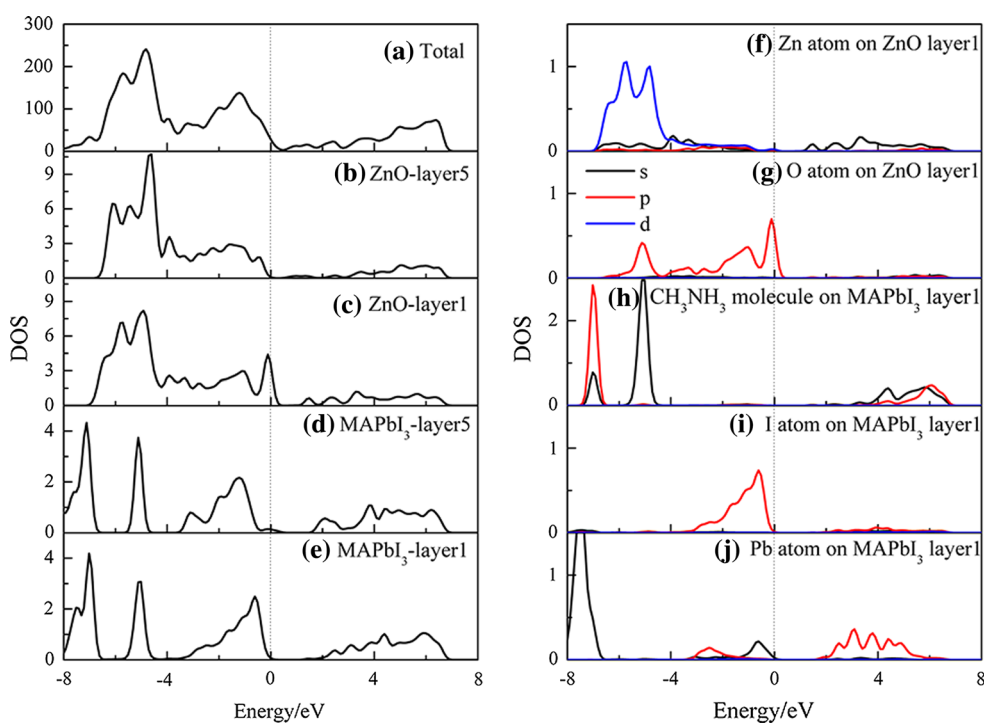

Figure 7 The total density of states of WZ-ZnO (100)/ $MAPbI_3$ (112) interface (**a**); the local density of states of WZ-ZnO layer 5 (**b**) and layer 1 (**c**); the local density of states of $MAPbI_3$ layer 5 (**d**), layer 1 (**e**); the partial density of states of Zn (**f**), O (**g**), CH_3NH_3 (**h**), I (**i**), Pb (**j**) on the interface layer 1.

level. Figure 7d, e shows LDOS of the $MAPbI_3$ (112) layer 5 and layer 1; the LDOS of $MAPbI_3$ (112) layer 5 represents that of the bulk $MAPbI_3$. Through analyzing LDOS of $MAPbI_3$ (112) layer 5 and LDOS of $MAPbI_3$ (112) layer 1, we find that $MAPbI_3$ (112) layer 1 also has some new energy densities states from −1.0 to 0 eV near the Fermi level. Through above analyzing LDOS of the WZ-ZnO (100) layer 1 and $MAPbI_3$ (112) layer 1, it can be seen that WZ-ZnO (100) layer 1 and $MAPbI_3$ (112) layer 1 have interface states from −1.0 to 0 eV and from −0.5 to 0.3 eV, respectively.

In order to further study the WZ-ZnO (100)/$MAPbI_3$ (112) interface, we give PDOS of the interface system. Figure 7f–j shows PDOS of the Zn, O, CH_3-NH_3, I, Pb atoms of layer 1 on the WZ-ZnO (100)/$MAPbI_3$ (112) interface. From Fig. 7f and g, it can be seen that the contribution to interface states of WZ-ZnO (100) layer 1 comes from O-2*p* orbital on WZ-ZnO (100) layer 1 from −0.5 to 0.3 eV. From −6 to −4 eV, the hybridizations of Zn-3*d* orbital and O-2*p* orbital are found through comparing Fig. 7f with g. Through analyzing Fig. 7h with j, we can see that the contribution to interface states of $MAPbI_3$ (112) layer 1 comes from I-5*p* orbital and Pb-6*s* orbital on $MAPbI_3$ (112) layer 1 from −1.0 to 0 eV. From −3 to 0 eV, there are some hybridizations of O-2*p* orbital, I-5*p* orbital, Pb-6*s* orbital with Pb-6*p* orbital through comparing Fig. 7f with j.

Figure 8a–j shows PDOS of Zn1–Zn6 atoms, O*x* ($x = 1$–6) atoms, I1–I3 atoms. As shown in Fig. 7c, f, we find that the contribution to new electronic states of WZ-ZnO (100) layer 1 comes from Zn atoms on WZ-ZnO (100) layer 1 from 1.0 to 3.0 eV. From Fig. 8a–f, it can be seen that these new electronic states are derived from 4*s*-orbital of Zn2 atom, Zn4 atom and Zn6 atom on WZ-ZnO (100) layer 1. This is mainly due to the influence of H atoms of CH_3NH_3 ion [48]. The contribution of 2*p*-orbital of O1–O6 atoms to interface states is almost the same in Fig. 8g. From Fig. 8h–j, we find that the contribution of 5*p*-orbital of I1 and I2 atoms to interface states is almost the same and the contribution of 5*p*-orbital of I3 atom to interface states is greater.

Table 1 shows the WZ-ZnO/$MAPbI_3$ interfacial electron numbers which have contribution to interface states. We find that O1, O2, O3, O4, O5, O6 atoms of the WZ-ZnO bulk have the same electron numbers of 7.28*e*, while O1, O2, O4 atoms of the WZ-ZnO layer 1 have the same electron numbers of 7.17*e*, O3, O6 atoms of the WZ-ZnO layer 1 have the same electron numbers of 7.19*e*, O5 atom of the WZ-ZnO layer 1 has electron numbers of 7.20*e*. Electron numbers of O atoms on the layer 1 are less than those in the bulk. Zn2, Zn4, Zn6 atoms of the WZ-ZnO bulk have the same electron numbers of 10.72*e*, while Zn2, Zn4, Zn6 atoms of the WZ-ZnO layer 1 have the electron numbers of 10.80*e*, 10.81*e*, 10.83*e*, respectively.

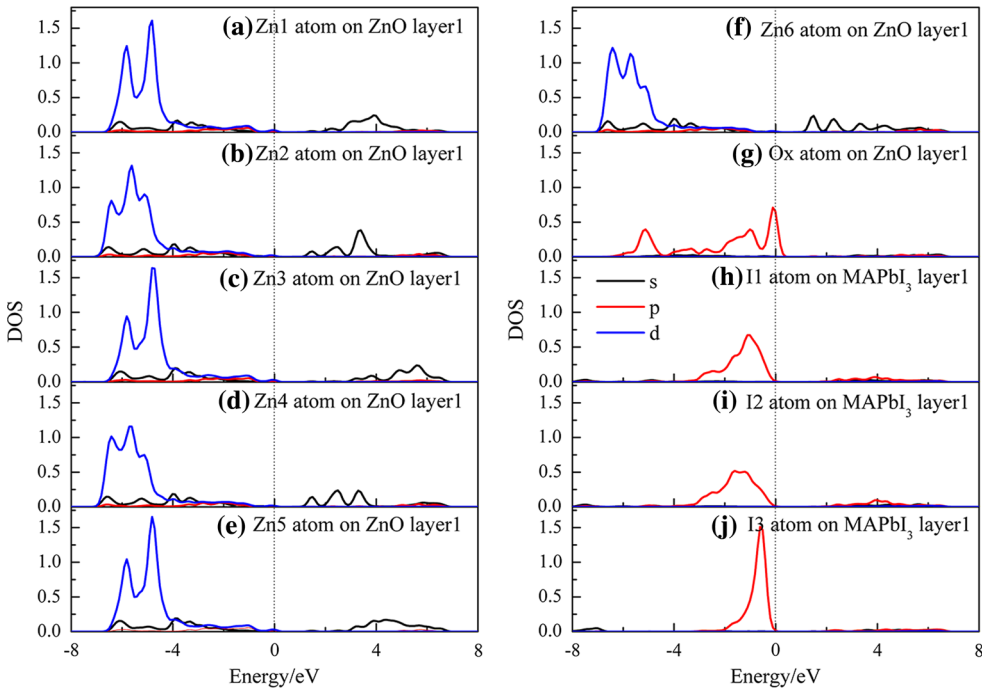

Figure 8 The partial density of states of Zn1 (**a**), Zn2 (**b**), Zn3 (**c**), Zn4 (**d**), Zn5 (**e**), Zn6 (**f**), O*x* ($x = 1$–6) (**g**) atoms on the WZ-ZnO layer 1, I1 (**h**), I2 (**i**), I3 (**j**) atoms on the $MAPbI_3$ layer 1.

Table 1 The electron numbers of $MAPbI_3$ layer 1 and WZ-ZnO layer 1 atoms contributing to the interface states

System	O1, O2, O4	O3, O6	O5	Zn2	Zn4	Zn6
Bulk of WZ-ZnO	7.28	7.28	7.28	10.72	10.72	10.72
WZ-ZnO layer 1	7.17	7.19	7.20	10.80	10.81	10.83

	I1	I2	I3	Pb
Bulk of $MAPbI_3$	7.57	7.57	7.57	13.06
$MAPbI_3$ layer 1	7.44	7.45	7.56	13.04

Electron numbers of Zn atoms on the layer 1 are greater than those is the bulk. I1, I2, I3 atoms of the $MAPbI_3$ bulk have the same electron numbers of 7.57*e*, while I1, I2, I3 atoms of the $MAPbI_3$ layer 1 have the electron numbers of 7.44*e*, 7.45*e*, 7.56*e*, respectively. Pb atom of the $MAPbI_3$ bulk has the electron numbers of 13.06*e*, and the electron numbers of Pb atom on the $MAPbI_3$ layer 1 are 13.04*e*. Electron numbers of I and Pb atoms on the layer 1 also are less than those in the bulk.

In order to better analyze electronic properties of WZ-ZnO (100)/$MAPbI_3$ (112) interface, we investigate charge density difference of the WZ-ZnO/$MAPbI_3$ interface system. Equation (6) gives the charge density difference

$$\Delta\rho = \rho_{\mathrm{WZ-ZnO/MAPbI3}} - \rho_{\mathrm{WZ-ZnO}} - \rho_{\mathrm{MAPbI3}} \quad (6)$$

Here, $\Delta\rho$ is the charge density difference, $\rho_{\mathrm{WZ\text{-}ZnO/MAPbI3}}$ describes the total charge density difference of interface system, and $\rho_{\mathrm{WZ\text{-}ZnO}}$ or ρ_{MAPbI3} is the charge density difference of isolated WZ-ZnO or $MAPbI_3$ slab of interface system.

The charge density difference of the WZ-ZnO (100)/$MAPbI_3$ (112) interface is shown in Fig. 9. Figure 9b is the partial enlarged view of Fig. 9a. The electrons obtained show yellow color, and the electrons loss shows blue–green color. As shown in Fig. 9, the charges redistribute between interfacial atoms. From Fig. 9, we can see that there are some charges transferred near the WZ-ZnO (100)/$MAPbI_3$ (112) interface. Charges transfer of the atoms near the interface is more than that of the atoms far from the interface. This charges transfer will promote the different atoms binding near the interface.

We use the Bader charges to quantitatively analyze the charge transfer. The Bader atomic charges in WZ-ZnO bulk, $MAPbI_3$ bulk, WZ-ZnO layer 1 and $MAPbI_3$ layer 1 of the interface are shown in Table 2. The WZ-ZnO bulk has 2 Zn atoms and 2 O atoms, and our calculation results show that two Zn atoms lose the same charges about 1.28*e*. The other two O atoms get the same charges about 1.28*e*. The $MAPbI_3$ bulk includes 1 CH_3NH_3 ion, 1 Pb atom, 3 I atoms. The results indicate that 1 CH_3NH_3 ion loses charges 0.77e. One Pb atom loses charges 1.12*e*. Every I atom gets charge 0.63*e*. WZ-ZnO layer 1 has 6 Zn atoms and 6 O atoms. Six Zn atoms on WZ-ZnO layer 1 lose charges about 1.21*e*, 1.20*e*, 1.15*e*, 1.19*e*, 1.17*e*, 1.17*e*, respectively. Six O atoms on WZ-ZnO layer 1 get charges about 1.17*e*, 1.17*e*, 1.19*e*, 1.17*e*, 1.20*e*, 1.19*e*, respectively. $MAPbI_3$ layer 1 has 1 CH_3NH_3 ion, 1 Pb atom and 3 I atoms. One CH_3NH_3 ion on the $MAPbI_3$ layer 1 loses 0.76*e*, 1 Pb atom on the $MAPbI_3$ layer 1 loses 0.96*e*, and 3 I atoms on the $MAPbI_3$ layer 1 get charges about 0.44*e*, 0.45*e*, 0.55*e*, respectively.

Above calculations indicate that WZ-ZnO/$MAPbI_3$ interface has interface states nearby the Fermi level. These interface states can affect the generation and recombination of carriers at the interface. The distribution of electrons in the interface state determines the position where the energy level is filled by electrons (relative Fermi level E_F). Different materials forming the interface may appear lattice discrepancies, and these discrepancies lead to incomplete bonding, that is, dangling bonds at the interface. Finally, the interface defect states appear at the interface. The multiple interfaces in the perovskite solar cells, also owing to the damage of the periodical structure at the interface, introduce a large number of interface states at the interface. These interface states can reduce the PCE of the perovskite solar cells.

Conclusions

In conclusion, the first-principles calculations were utilized to investigate optical properties and electronic properties of the WZ-ZnO/$MAPbI_3$ interface. The optical band gap of bulk $MAPbI_3$ is about 1.81 eV, corresponding to electron transitions from

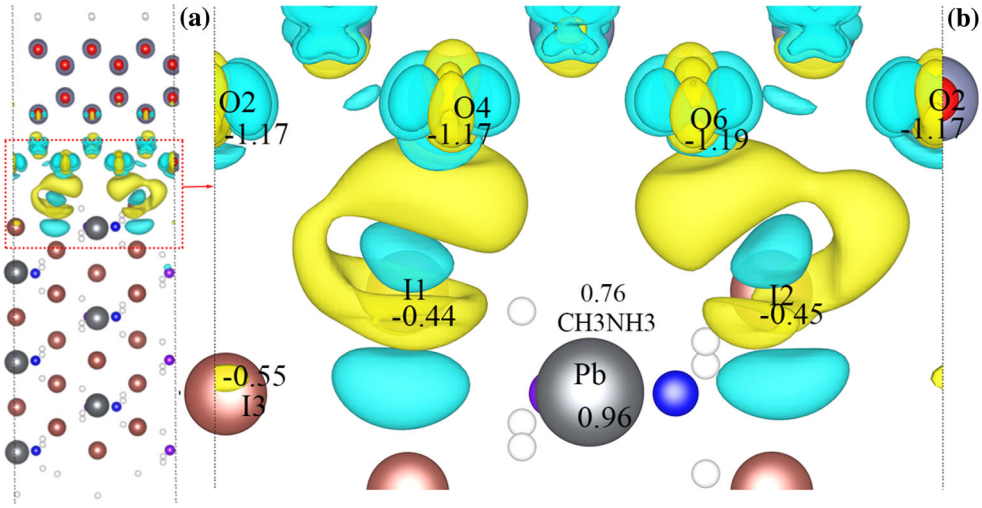

Figure 9 The density charge difference (**a**), partial enlarged view (**b**) of the WZ-ZnO (100)/$MAPbI_3$ (112) interface.

Table 2 Bader atomic charges of bulk WZ-ZnO and $MAPbI_3$, WZ-ZnO layer 1 and $MAPbI_3$ layer 1 of the interface

System	CH_3NH_3	Pb	I	Zn	O
Bulk of $MAPbI_3$	0.77	1.12	−0.63		
Bulk of WZ-ZnO				1.28	−1.28
$MAPbI_3$ layer 1	0.76	0.96	−0.55 to −0.44		
WZ-ZnO layer 1				1.15–1.21	−1.20 to −1.17

the O-2*p* orbitals in valence bands to the Pb-6*p* orbitals in conduction bands. Compared with optical properties of the $MAPbI_3$ bulk, the absorption coefficient, refractive indices and extinction coefficient of the $MAPbI_3$ surface or WZ-ZnO/$MAPbI_3$ interface are reduced. The damage of periodical crystal at the surface or interface leads to such electronic property change. The interface states appear near the Fermi level, which come from the contribution of O-2*p* orbital, I-5*p* orbital and Pb-6*s* orbital nearby the interface. These interface states can affect the generation and recombination of carriers at the interface, and then, they do harm to the power conversion efficiency of the perovskite solar cells. From the quality of WZ-ZnO/$MAPbI_3$ interface, all of the above factors are unfavorable, showing that WZ-ZnO/$MAPbI_3$ interface is not an ideal interface for such solar cell.

Acknowledgements

This work was financially supported by the National Natural Science Foundation of China (11764027 and 11364025). This work was performed in the Gansu Supercomputer Center. Tang was financially supported by Chinese Scholarship Council.

References

[1] Stranks SD, Eperon GE, Grancini G, Menelaou C, Alcocer MJ, Leijtens T, Herz LM, Petrozza A, Snaith HJ (2013) Electron–hole diffusion lengths exceeding 1 micrometer in an organometal trihalide perovskite absorber. Science 342:341–344

[2] Yin WJ, Shi TT, Yan YF (2014) Unusual defect physics in $CH_3NH_3PbI_3$ perovskite solar cell absorber. Appl Phys Lett 104:063903

[3] Gottesman R, Haltzi E, Gouda L, Tirosh S, Bouhadana Y, Zaban A (2014) Extremely slow photoconductivity response of $CH_3NH_3PbI_3$ perovskites suggesting structural changes under working conditions. J Phys Chem Lett 5:2662–2669

[4] Xing GC, Mathews N, Sun SY, Lim SS, Lam YM, Grätzel M, Mhaisalkar S, Sum TC (2013) Long-range balanced electron- and hole-transport lengths in organic–inorganic $CH_3NH_3PbI_3$. Science 342(6156):344–347

[5] Grätzel M (2014) The light and shade of perovskite solar cells. Nat Mater 13:838–842

[6] Dar MI, Arora N, Gao P, Ahmad S, Grätzel M, Nazeeruddin MK (2014) Investigation regarding the role of chloride in organic–inorganic halide perovskites obtained from chloride containing precursors. Nano Lett 14:6991–6996

[7] Kim HS, Im SH, Park NG (2014) Organolead halide perovskite: new horizons in solar cell research. J Phys Chem C 118(11):5615–5625

[8] Dequilettes DW, Vorpahl SM, Stranks SD, Naqaoka H, Eperon GE, Ziffer ME, Snaith HJ, Ginqer DS (2015) Solar cells. Impact of microstructure on local carrier lifetime in perovskite solar cells. Science 348:683–686

[9] Kagan CR, Mitzi DB, Dimitrakopoulos CD (1999) Organic–inorganic hybrid materials as semiconducting channels in thin-film field-effect transistors. Science 286:945–947

[10] Liu DY, Kelly TL (2014) Perovskite solar cells with a planar heterojunction structure prepared using room-temperature solution processing techniques. Nat Photonics 8:133–138

[11] Ku Z, Rong Y, Xu M, Liu T, Han H (2013) Full printable processed mesoscopic $CH_3NH_3PbI_3/TiO_2$ heterojunction solar cells with carbon counter electrode. Sci Rep 3:3132

[12] Kojima A, Teshima K, Shirai Y, Miyasaka T (2009) Organometal halide perovskites as visible-light sensitizers for photovoltaic cells. J Am Chem Soc 131:6050–6051

[13] Wojciechowski K, Saliba M, Leijtens T, Abate A, Snaith HJ (2014) Sub-150 °C processed meso-superstructured perovskite solar cells with enhanced efficiency. Energy Environ Sci 7(3):1142–1147

[14] Kojima A, Teshima K, Shirai Y, Miyasaka T (2006) Novel photoelectrochemical cell with mesoscopic electrodes sensitized by lead-halide compounds (2). In: ECS meeting, p 397

[15] Wang KC, Shen PS, Li MH, Chen S, Lin MW, Chen P, Guo TF (2014) Low-temperature sputtered nickel oxide compact thin film as effective electron blocking layer for mesoscopic $NiO/CH_3NH_3PbI_3$ perovskite heterojunction solar cells. ACS Appl Mater Interfaces 6(15):11851–11858

[16] Wang JJ, Wang SR, Li XG, Zhu LF, Meng QB, Xiao Y, Li DM (2014) Novel hole transporting materials with a linear pi-conjugated structure for highly efficient perovskite solar cells. Chem Commun 50:5829–5832

[17] Shi JJ, Xu X, Li DM, Meng QB (2015) Interfaces in perovskite solar cells. Small 11(21):2472–2486

[18] Yang JL, Siempelkamp BD, Mosconi E, Angelis FD, Kelly TL (2015) Origin of the thermal instability in $CH_3NH_3PbI_3$ thin films deposited on ZnO. Chem Mater 27(12):4229–4236

[19] Zhou XZ, Li XL, Liu Y, Huang F, Zhong DY (2016) Interface electronic properties of co-evaporated $MAPbI_3$ on ZnO (0001): in situ X-ray photoelectron spectroscopy and ultraviolet photoelectron spectroscopy study. Appl Phys Lett 108(12):121601

[20] Zhang JH, Li FS, Yang KY, Veeramalai CP, Guo TL (2016) Low temperature processed planar heterojunction perovskite solar cells employing silver nanowires as top electrode. Appl Surf Sci 369:308–313

[21] Zhou HW, Shi YT, Wang K, Dong QS, Bai XG, Xing YJ, Du Y, Ma TL (2015) Low-temperature processed and carbon-based $ZnO/CH_3NH_3PbI_3/C$ planar heterojunction perovskite solar cells. J Phys Chem C 119(9):4600–4605

[22] Song JX, Bian J, Zheng EQ, Wang XF, Tian WJ, Miyasaka T (2015) Efficient and environmentally stable perovskite solar cells based on ZnO electron collection layer. Chem Lett 44(5):610–612

[23] Son DY, Im JH, Kim HS, Park NG (2014) 11% Efficient perovskite solar cell based on ZnO nanorods: an effective charge collection system. J Phys Chem C 118(30):16567–16573

[24] Kresse G, Furthmüller J (1996) Efficiency of ab initio total energy calculations for metals and semiconductors using a plane-wave basis set. Comput Mater Sci 6(1):15–50

[25] Kresse G, Furthmüller J (1996) Efficient iterative schemes for ab initio total-energy calculations using a plane-wave basis set. Phys Rev B 54(16):11169–11186

[26] Yu J, Lin X, Wang JJ, Chen J, Huang WD (2009) First-principles study of the relaxation and energy of bcc-Fe, fcc-Fe and AISI-304 stainless steel surfaces. Appl Surf Sci 255(22):9032–9039

[27] Perdew JP, Burke K, Ernzerhof M (1996) Generalized gradient approximation made simple. Phys Rev Lett 77(18):3865–3868

[28] Ma LC, Zhang JM, Xu KW (2013) Magnetic and electronic properties of Fe/Cu multilayered nanowires: a first-principles investigation. Physica E 50:1–5

[29] Kresse G, Joubert D (1999) From ultrasoft pseudopotentials to the projector augmented-wave method. Phys Rev B 59(3):1758–1775

[30] Gajdoš M, Hummer K, Kresse G (2006) Linear optical properties in the projector-augmented wave methodology. Phys Rev B 73(4):045112

[31] Mulliken RS (1955) Electronic population analysis on LCAO–MO molecular wave functions. J Chem Phys 23:1833–1840

[32] Bader RFW (1990) Atoms in molecules: a quantum theory. Oxford University Press, New York

[33] Henkelman G, Arnaldsson A, Jónsson H (2006) A fast and robust algorithm for Bader decomposition of charge density. Comput Mater Sci 36(3):354–360

[34] Momma K, Izumi F (2008) VESTA: a three-dimensional visualization system for electronic and structural analysis. J Appl Cryst 41:653–658

[35] Cheng YW, Tang FL, Xue HT, Liu HX, Gao B, Feng YD (2016) First-principles study on electronic properties and lattice structures of WZ-ZnO/CdS interface. Mat Sci Semicon Proc 45:9–16

[36] Weber D (1978) $CH_3NH_3PbX_3$, ein Pb(II)-system mit kubischer perowskitstruktur/$CH_3NH_3PbX_3$, a Pb(II)-system with cubic perovskite structure. Z Naturforsch B 33(12):1443–1445

[37] Poglitsch A, Weber D (1987) Dynamic disorder in methylammoniumtrihalogenoplumbates (II) observed by millimeter-wave spectroscopy. J Chem Phys 87(11):6373–6378

[38] Kawamura Y, Mashiyama H, Hasebe K (2002) Structural study on cubic-tetragonal transition of $CH_3NH_3PbI_3$. J Phys Soc Jpn 71:1694–1697

[39] Onoda-Yamamuro N, Matsuo T, Suga H (1990) Calorimetric and IR spectroscopic studies of phase transitions in methylammonium trihalogenoplumbates (II). J Phys Chem Solids 51(12):1383–1395

[40] Zhou JG, Causon DM, Mingham CG, Ingram DM (2001) The surface gradient method for the treatment of source terms in the shallow-water equations. J Comput Phys 168(1):1–25

[41] Blöchl PE, Jepsen O, Andersen OK (1994) Improved tetrahedron method for Brillouin-zone integrations. Phys Rev B 49(23):16223–16233

[42] Cheng YW, Tang FL, Xue HT, Liu HX, Gao B, Feng YD (2016) Bonding and electronic properties of the Cu_2ZnSnS_4/WZ–ZnO interface from first-principles calculations. J Phys D Appl Phys 49(28):285107–285117

[43] Liu HX, Tang FL, Xue HT, Zhang Y, Cheng YW, Feng YD (2016) Lattice structures and electronic properties of WZ-$CuInS_2$/WZ-CdS interface from first-principles calculations. Chin Phys B 25(12):211–220

[44] Leguy AMA, Azarhoosh P, Alonso MI, Campoy-Quiles M, Weber OJ, Yao JZ, Bryant D, Weller MT, Nelson J, Walsh A, Schilfgaarde MV, Barnes PRF (2016) Experimental and theoretical optical properties of methylammonium lead halide perovskites. Nanoscale 8:6317–6327

[45] Green MA, Jiang YJ, Soufiani AM, Ho-Baillie A (2015) Optical properties of photovoltaic organic–inorganic lead halide perovskites. J Phys Chem Lett 6:4774–4785

[46] Umari P, Mosconi E, De Angelis F (2014) Relativistic GW calculations on $CH_3NH_3PbI_3$ and $CH_3NH_3SnI_3$ perovskites for solar cell applications. Sci Rep 4(3):4467

[47] Xie ZA, Liu SF, Qin LX, Pang SP, Wang W, Yan Y, Yao L, Chen ZJ, Wang SF, Du HL, Yu MH, Qin GG (2015) Refractive index and extinction coefficient of $CH_3NH_3PbI_3$ studied by spectroscopic ellipsometry. Opt Mater Express 5(1):29–43

[48] Ozawa K, Mase K (2011) Comparison of the surface electronic structures of H-adsorbed ZnO surfaces: an angle-resolved photoelectron spectroscopy study. Phys Rev B 83(12):5121–5124